Theoretical aspects of the 3-D ZO CRS stack

Pedro Chira-Oliva(*), João C. R. Cruz(*), Peter Hubral(†) and Martin Tygel (‡)

(*) Federal University of Pará (Brazil), chira, jcarlos@ufpa.br

(†) Geophysical Institute of Karlsruhe (Germany), peter.hubral@gpi.uni-karlsruhe.de

(‡) LGC, State University of Campinas (Brazil), tygel@ime.unicamp.br

This paper was prepared for presentation at the 8th International Congress of The Brazilian Geophysical Society held in Rio de Janeiro, Brazil, 14-18 September 2003.

Abstract

We present some new theoretical aspects of the 3-D Common-Reflection-Surface (CRS) stack to simulate zero-offset (ZO) volume from pre-stack seismic data. The CRS method is based on the second-order hyperbolic approximation of the reflection traveltime in the vicinity of a central ray. The hyperbolic traveltime expression depends on eight parameters that are estimated by means of a coherence analysis procedure. After an optimization process, the estimated CRS parameters are substituted in the hyperbolic traveltime and applied to stack the multi-coverage seismic data providing a high-resolution ZO volume. The optimized CRS parameters can also be used for a number of applications. These include interval velocity inversion, computation of geometrical spreading factors and projected Fresnel zones, and time and depth migration schemes.

Introduction

3-D seismic surveys are at present major tools in hydrocarbons exploration and exploitation (Walton, 1972). The first 3-D seismic survey was carried out in the late 1970s. In 1975, 3-D surveys were first performed on a normal contractual basis. Bone et al. (1976) showed the new technology to the world. The scope of 3-D seismic for field development was firstly reported by Tegland (1977). But it took until the early 1990s before they gained general acceptance throughout the industry.

The essence of the 3-D method is an areal data collection followed by processing and interpretation of a data volume. 3-D surveys provide more details of the subsurface and contribute significantly to the problems of field appraisal, development, production and exploration. The fundamental objective of the 3-D seismic method is an increased resolution.

In order to overcome a number of limitations of the NMO-method, so as to improve seismic-imaging results, so-called model-independent methods have been introduced. The Common-Reflection-Surface (CRS) stack is one of these new methods. For a survey on model-independent methods, the reader is referred to Hubral (1999). The CRS method uses the second-order paraxial approximation of the reflection traveltime to simulate ZO sections (ZO-CRS stacks) and common-offset (CO) sections (CO-CRS stacks). The resulting stacked sections are characterized by an increased signal-to-noise ratio and improved lateral resolution of the stacked volume. In the ZO case, the 3-D traveltime formula depends on eight parameters, that are determined by a multi-parametric optimization procedure. An impressive example of 3-D CRS stack application is given by Bergler et al. (2002).

In this paper, we examine the 3-D CRS traveltime formula in the framework to its application to construct a simulated ZO volume by a stacking procedure carried out on a 3-D pre-stack seismic data. We also present some applications that result from the knowledge of the estimated 3-D CRS parameters.

3-D ZO CRS stacking operator for reflections events

We consider an arbitrary 3-D layered model below a planar measurement surface (Figure 1). In this model, we consider a fixed primary ZO reflection ray, called the central ray. Its coincident source-receiver pair at the measurement surface, called the central point, is denoted by X_0. The traveltime of the ZO central ray is denoted by t_0. A fixed 2-D Cartesian coordinate system on the planar horizontal measurement surface and with origin at the central point, X_0, is used to locate all sources, $\mathbf{s} = (x_S, y_S)$, and receivers, $\mathbf{g} = (x_G.y_G)$ on that surface. Source and receiver pairs, $(\mathbf{s}, \mathbf{g})$, can be conveniently located by means of midpoint and half-offset coordinates, $(\mathbf{x}_m, \mathbf{h})$, defined by $\mathbf{x}_m = (1/2)(x_G + x_S, y_G + y_S)$ and $\mathbf{h} = (1/2)(x_G - x_S, y_G - y_S)$, respectively (see Figure 2).

For a primary reflection ray that connects a source and receiver pair, (S, G) in the vicinity of the central point, X_0, we can express its hyperbolic traveltime approximation in the form (see, e.g., Bortfeld (1989);Schleicher et al. (1993))

$$\begin{aligned} t^2(\mathbf{x}_m, \mathbf{h}) = &(t_0 + 2\,\mathbf{p}_0 \cdot \mathbf{x}_m)^2 \\ &+ 2\,t_0\,\mathbf{x}_m \cdot \mathbf{D_0}^{-1}\,\mathbf{C_0}\,\mathbf{x}_m \\ &+ 2\,t_0\,\mathbf{h} \cdot \mathbf{B_0}^{-1}\,\mathbf{A_0}\,\mathbf{h}\,. \end{aligned} \tag{1}$$

Here, $\mathbf{p}_0 = (\partial t/\partial \mathbf{x}_m)/2$ is the horizontal projection of the slowness vector of the normal (central) ray at X_0 with respect to the measurement surface. Moreover,

$$\mathbf{D_0}^{-1}\,\mathbf{C_0} = \frac{1}{2}\frac{\partial^2 t}{\partial \mathbf{h}^2}, \quad \mathbf{B_0}^{-1}\,\mathbf{A_0} = \frac{1}{2}\frac{\partial^2 t}{\partial \mathbf{x}_m^2}\,, \tag{2}$$

are 2×2 second-derivative (Hessian) matrices also evaluated at X_0. We recall that $\mathbf{A_0}, \mathbf{B_0}, \mathbf{C_0}$ and $\mathbf{D_0}$ represent

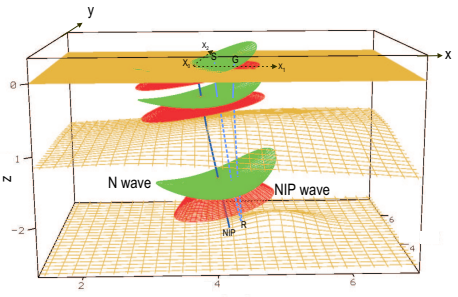

Figure 1: 3-D model constituted of two isovelocity layers with curved interfaces above a dome-like half-space. The normal (central) ray $X_0\ NIP\ X_0$ is plotted in red and describes the direction of propagation of the NIP and N hypothetical wavefronts. The paraxial ray SRG is depicted in green. (x, y, z) is the global cartesian coordinates system (modified from Höcht (2002)).

the (constant) 2×2 submatrices of the 4x4 propagator matrix $\mathbf{T_0}$, that characterize the one-way normal ray from the normal-incident-point (NIP) of the central ray to the measurement surface (Bortfeld (1989); Hubral et al. (1992)). Introducing the notation $\mathbf{D_0}^{-1}\mathbf{C_0} = \mathbf{A}/v_1$, $\mathbf{B_0}^{-1}\mathbf{A_0} = \mathbf{B}/v_1$ and $\mathbf{p_0} = \mathbf{c}/v_1$ in eq. (1), where v_1 is the medium velocity at the central point, equation (1) can be recast as

$$t^2(\mathbf{x}_m, \mathbf{h}) = \left(t_0 + \frac{2}{v_1}\,\mathbf{c}\,\cdot\,\mathbf{x}_m\right)^2 + \frac{2\,t_0}{v_1}\,\mathbf{x}_m\cdot\,\mathbf{A}\,\mathbf{x}_m + \frac{2\,t_0}{v_1}\,\mathbf{h}\cdot\,\mathbf{B}\,\mathbf{h}\,. \tag{3}$$

Following Hubral et al. (1991) and Chira (2003) we can also write

$$\mathbf{A} = \mathbf{D}_{zy}\,\mathbf{N}\,\mathbf{D}_{zy}^T \quad \text{and} \quad \mathbf{B} = \mathbf{D}_{zy}\,\mathbf{M}\,\mathbf{D}_{zy}^T, \tag{4}$$

where $\mathbf{D}_{zy}$ is the 2-D transformation matrix (Jäger, 1999)

$$\mathbf{D}_{zy} = \mathbf{D}_z\,(\varphi_1)\,\mathbf{D}_y\,(\varphi_2)\,, \tag{5}$$

in which

$$\begin{aligned} \mathbf{D}_z\,(\varphi_1) &= \begin{pmatrix} \cos\varphi_1 & -\sin\varphi_1 \\ \sin\varphi_1 & \cos\varphi_1 \end{pmatrix}, \\ \mathbf{D}_y\,(\varphi_2) &= \begin{pmatrix} \cos\varphi_2 & 0 \\ 0 & 1 \end{pmatrix}. \end{aligned} \tag{6}$$

are rotation matrices.

The superscript T denotes transposition. $\mathbf{A}$ and $\mathbf{B}$ are symmetric 2×2 matrices that represent the second-order derivatives of the traveltime t with respect to midpoint and half-offset coordinates times the velocity v_1. $\mathbf{c}$ is the ground surface projection vector of the normal ray direction 3-D vector at X_0. φ_1 and φ_2 describe the azimuth and polar angle of the normal ray direction. $\mathbf{M}$ and $\mathbf{N}$ are symmetric 2×2 curvature matrices of the Normal-Incidence-Point (NIP) and Normal (N) waves (Hubral, 1983). The 3-D CRS

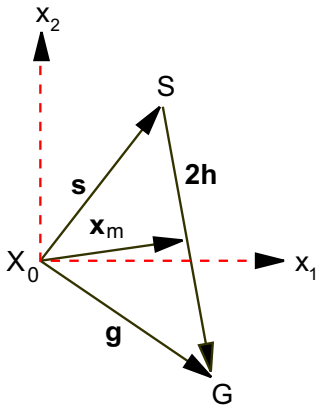

Figure 2: Definition of midpoint $\mathbf{x}_m$ and half-offset $\mathbf{h}$ vectors on the planar measurement surface. $\mathbf{s}$ and $\mathbf{g}$ denote the shot and receiver vectors originated at the point X_0. (x_1, x_2) is the local Cartesian coordinates system centered at point X_0.

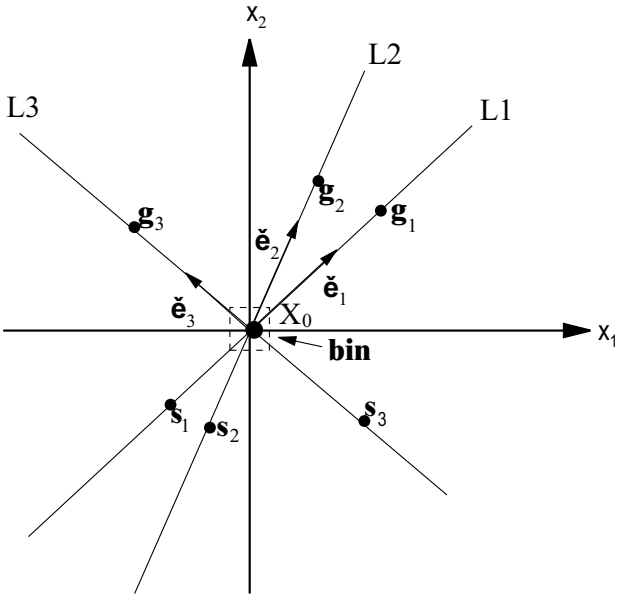

Figure 3: Three seismic lines L1, L2, e L3 intersecting at point X_0 in the local (x_1, x_2) Cartesian coordinate system. They define the directions of unitary vectors $\check{\mathbf{e}}_i$ $(i = 1, 2, 3)$. $\mathbf{s}_i$, $\mathbf{g}_i$ are the shot and receiver coordinates on three seismic pseudo-lines.

stacking operator (equation 3) depends on eight parameters: 3 parameters from matrix $\mathbf{A}$, 3 parameters from matrix $\mathbf{B}$ and 2 from vector $\mathbf{c}$.

We now discuss two important simplifications of the move-out formula (3), that are part of the search strategy for estimating its eight CRS parameters at X_0.

CMP gather

For a Common-Midpoint (CMP) gather, the source $\mathbf{s}$ is located opposite to the receiver $\mathbf{g}$ with respect to the central point X_0 (Figure 3), namely $\mathbf{s} = -\mathbf{g}$. In midpoint and half-offset co-ordinates and assuming the CMP at the origin, we have the simple condition $\mathbf{x}_m = 0$. Equation (3), then, reduces to

$$t_{CMP}^2 = t_0^2 + \frac{2\,t_0}{v_1}\ \mathbf{h}\ \cdot\ \mathbf{B}\ \mathbf{h}. \qquad (7)$$

Matrix $\mathbf{V}$ is interpreted as the inverse square NMO velocity matrix given by

$$\mathbf{V} = \frac{t_0\,\mathbf{B}}{2\,v_1}. \qquad (8)$$

ZO gather

In the case of a ZO configuration, the coincident source and receiver pairs in the ZO gather are easily described by the condition $\mathbf{s} = \mathbf{g}$, or $\mathbf{h} = 0$ in midpoint and half-offset co-ordinates. Substituting into equation (3), we find

$$t_{ZO}^2(\mathbf{x}_m) = \left(t_0 + \frac{2}{v_1}\,\mathbf{c}\cdot\mathbf{x}_m\right)^2 + \frac{2\,t_0}{v_1}\,\mathbf{x}_m\ \cdot\mathbf{A}\ \mathbf{x}_m. \qquad (9)$$

The 3-D ZO CRS method has been already successfully applied both to synthetic (Cristini et al., 2001) and real datasets (Bergler et al., 2002). In Chira (2003), some strategies to estimate CRS eight parameters have been proposed.

3-D ZO CRS stacked volume

The first application of the 3-D ZO CRS stack on synthetic dataset was carried out by ENI Division (AGIP-Italy) (Cristini et al., 2001) with impressive results.

First results on the 3-D ZO CRS stack were obtained by ENI Division (AGIP-Italy) using synthetic datasets. The reader is referred to Cristini et al. (2001) for more details concerning the strategy applied for this stack. The considered model is the one shown in Figure 4. It is a 3-D acoustic model consisting of two isovelocity layers with curved interfaces above a dome-like half-space. A conventional acquisition scheme has been applied. Bin size (Figure 3) is 0.025 x 0.025 km2, with 0.0125 and 3.5 kms being the minimum and maximum offsets obtained with a cross-shooting technique with 10 receivers cables by 96 channels. The primary reflection responses have been generated using the seismic package NORSAR 3-D, with a 20 Hz zero-phase Ricker wavelet.

Figure 5 results from the application of the 3-D CMP stack. This (conventional) process only considers 3-D CMP gathers. Figure 6 shows the result of the 3-D CRS ZO stacking

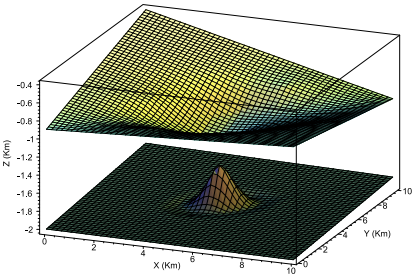

Figure 4: 3-D model constituted of two constant velocity layers above a dome-like half-space. The velocities are, 2, 3 and 5 km/s, respectively.

operation applied to the previous 3-D CMP stack. Finally, Figure 7 shows the 3-D CRS ZO stack applied to the full multicoverage pre-stack seismic data computed from the model of Figure 4. Note the good recovery of the events in their correct positions.

Further applications

Estimation of ZO geometrical spreading factors

For a point-source excitation in a 3-D homogeneous medium, a spherical wavefront propagates through the medium without any intrinsic attenuation. The so-called spherical divergence accounts for the amplitude loss that occurs because of the expanding wavefront. The amplitude change is inverse proportional to the radius of curvature of the propagating wavefront. In the case of propagation in an inhomogeneous layered medium, the wavefront are no longer spherical. Accordingly, the term geometrical spreading (GS) replaces the previously used spherical divergence.

According to ray theory, the GS factor can be accounted for by a factor L that appears in denominator of expression of amplitude. The GS has a major impact on the change in amplitude, in many case much more relevant than the ones caused by transmission through interfaces along the ray. As a consequence, correct elimination of the GS in the observed amplitudes can be essential for Amplitude versus Offset (AVO) or Amplitude versus Angle (AVA) studies. The term true-amplitude referred to a section in which the amplitudes have been corrected from their GS effects (Hubral, 1983). In this case, for primary reflections, these amplitudes can be interpreted as (scaled) measures of reflection coefficients, so that AVO or AVA is made possible.

As shown in Hubral (1983), the 3-D ZO GS factor L can be expressed as

$$L = \frac{2}{\sqrt{\det(\mathbf{M}-\mathbf{N})}}\,. \qquad (10)$$

Introducing equations (4) into equation (10), we find that L can be recast as

$$L = \frac{2}{\sqrt{\det(\mathbf{D}_{zy}^T\ \mathbf{B}\ \mathbf{D}_{zy} - \mathbf{D}_{zy}^T\ \mathbf{A}\ \mathbf{D}_{zy})}}\,. \qquad (11)$$

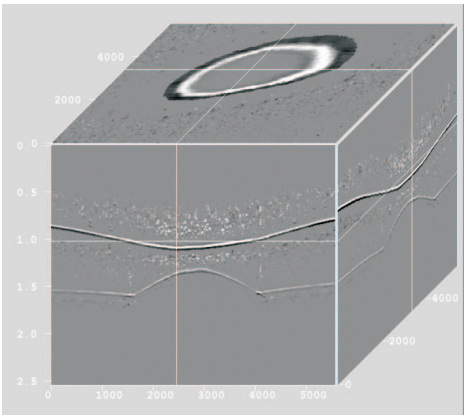

Figure 5: Volume obtained by applying the 3-D CMP stack referred to model of Figure 4. In this process was only considered the 3-D CMP gathers (Courtesy of AGIP).

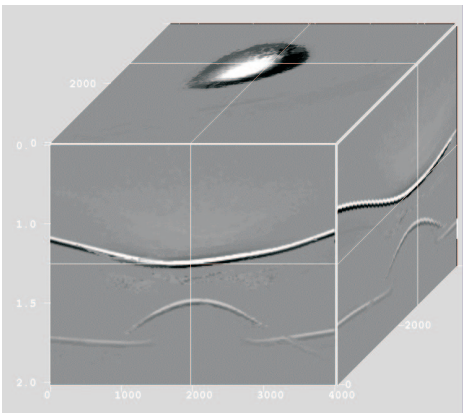

Figure 6: Volume obtained by applying the 3-D ZO stack from the result of the 3-D CMP stack (Courtesy of AGIP).

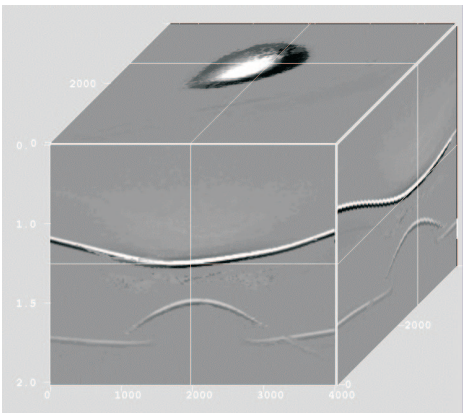

Figure 7: Simulated ZO volume by applying the 3-D ZO CRS stack method. This process considers all the multi-coverage seismic data from 3-D model (Figure 4) (Courtesy of AGIP).

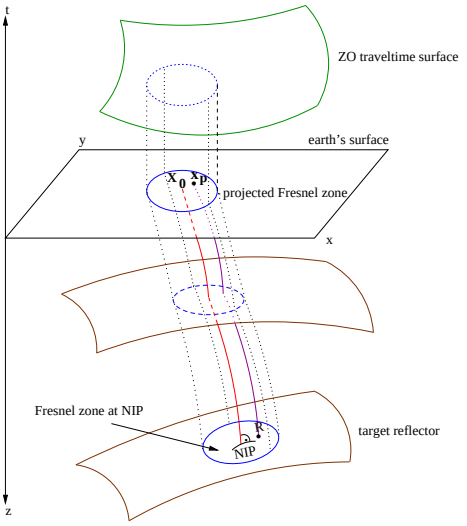

Figure 8: 3-D model with an arbitrary normal ray $x_p\ NIP\ x_p$. The 3-D Fresnel zone is shown at point NIP. Also is depicted the projected Fresnel zone onto the measurement surface and from there onto the traveltime surface (adapted from Hubral et al. (1993)).

Projected Fresnel zones

Images that result from Kirchhoff depth or time migration can are very affected by the choice of apertures that are used in the process. The best apertures are provided by the so-called Fresnel zone of the reflector to be imaged. In the ZO situation, the concept of a projected Fresnel zone has been introduced in Hubral et al. (1993). The projected Fresnel zone represents an optimum aperture for the stacking procedure. For the 3-D ZO CRS stacking operator of (equation 1) we use the projected Fresnel zone on the earth surface can be expressed as (see Hubral et al. (1993))

$$\left|\mathbf{x}_P \cdot \mathbf{H}_p \mathbf{x}_P\right| \leq \tau \ , \tag{12}$$

The vector $\mathbf{x}_P$ is the projected coordinate into the earth surface of a point in the vicinity of NIP on the reflector (Hubral et al. (1993), see Figure 8). τ is the period of the considered time-harmonic wave. Following Hubral et al. (1993) the projected Fresnel matrix $\mathbf{H}_p$ is given by

$$\mathbf{H}_p = 32\ \left[\mathbf{B}_0^{-1}\mathbf{A}_0 - \mathbf{D}_0^{-1}\mathbf{C}_0\right] \ . \tag{13}$$

Introducing the relationships for the 3-D ZO CRS stack operator, $\mathbf{D_0}^{-1}\mathbf{C_0} = \mathbf{A}/v_1$ and $\mathbf{B_0}^{-1}\mathbf{A_0} = \mathbf{B}/v_1$ (Chira, 2003) into equation (13) we obtain

$$\mathbf{H}_p = \frac{32}{v_1}\ \left[\mathbf{B} - \mathbf{A}\right] \ . \tag{14}$$

Finally, we include (14) into equation (12) for obtaining

$$\frac{32}{v_1}\left|\mathbf{x}_P \cdot \left[\mathbf{B} - \mathbf{A}\right]\mathbf{x}_P\right| \leq \tau \ . \tag{15}$$

Equation (15) can be considered as the initial aperture for the 3-D ZO CRS stacking operator of equation (3).

3-D ZO-CRS stacking operator for diffraction events

One of the important problems in the interpretation of seismic data is the identification of structural geologic feature (e.g. faults, pinch-outs, small-size scattering object). Local elements in the subsurface with a size comparable to the source wavelength are usually ignored by processing and are identified only during the interpretation process.

To obtain reliable information about possible discontinuities in the subsurface, the presence of diffracted waves, in the vicinity of the discontinuity location, is very important. The presence of diffracted waves in the multi-coverage prestack seismic data can be useful for detection of discontinuities.

In conventional seismic processing, diffracted waves are regarded as noise and the information contained in these waves has not been used. In the CRS method, however, attributes can be used to characterize diffraction events.

In the case of a diffraction point, the 3-D ZO diffracted traveltime can be formulated by setting the matrices $\mathbf{N} = \mathbf{M}$ or $\mathbf{A} = \mathbf{B}$ in equation (3). This yields

$$t^2_{diff}(\mathbf{x}_m, \mathbf{h}) = \left(t_0 + \frac{2}{v_1}\ \mathbf{c}\ \cdot\ \mathbf{x}_m\right)^2 + \frac{2\,t_0}{v_1}\ [\mathbf{x}_m \cdot\ \mathbf{B}\ \mathbf{x}_m] + \frac{2\,t_0}{v_1}\,[\mathbf{h} \cdot\ \mathbf{B}\ \mathbf{h}]\ . \tag{16}$$

The above equation depends on five parameters: two components of vector $\mathbf{c}$ and three elements of matrix $\mathbf{B}$. Chira (2003) also proposed some strategies to determine these parameters.

Conclusions

We have presented the formalism and examples of applications of the 3-D ZO CRS stacking operator for reflection events. This operator depends on eight search-parameters. We also proposed the 3-D ZO CRS stack operator for diffraction events which depends on five parameters. Both stacking operators are in fact valid for a 3-D laterally inhomogeneous velocity model and can be used to simulate a ZO volume from multi-coverage reflection prestack seismic data. We have shown special formulas for applications of the 3-D ZO CRS attributes to determine ZO geometrical spreading factors and ZO Projected Fresnel zones. The latter are important to define the aperture for stacking and migration.

Acknowledgments

The first author thanks to National Council of Technology and Development (CNPq) for the scholarship. We thank ENI- AGIP Division (Italy) for the permission to show the results of the 3-D ZO CRS stack. We also thank the support of the WIT Consortium.

References

Bergler, S., Hubral, P., Marchetti, P., Cristini, A., and Cardone, G., 2002, 3D common-reflection-surface stack and kinematic wavefield attributes: The Leading Edge, **21**, 1010–1015.

Bone, M. R., F., G. B., and Tegland, E. R., 1976, 3-D high resolution data collection, processing and display: 46th Annual Internat. Mtg., Soc. Expl. Geophys., Expanded Abstracts.

Bortfeld, R., 1989, Geometrical ray theory: Rays and traveltimes in seismic systems (second order approximation of the traveltimes): Geophysics, **1**, no. 54, 342–349.

Chira, P., 2003, Empilhamento pelo método Superfície de Reflexão Comum 2-D com Topografia e Introdução ao caso 3-D (in portuguese): Ph.D. thesis, Federal University of Para (Brazil).

Cristini, A., Cardone, G., Chira, P., Hubral, P., and Marchetti, 2001, 3D Zero-Offset Common Reflection Surface Stack for Land Data: 71th Annual Internat. Mtg., Soc. Expl. Geophys., Expanded Abstracts, Session W5–13.

Höcht, G., 2002, Traveltime approximation for 2D and 3D media and kinematic wavefield attributes.: Ph.D. thesis, University of Karlsruhe (Germany).

Hubral, P., Tygel, M., and Zien, H., 1991, Three-dimensional true-amplitude zero-offset migration: Geophysics, **56**, no. 1, 18–26.

Hubral, P., Schleicher, J., and Tygel, M., 1992, Three-dimensional paraxial ray properties, Part I: Basic relations: Journal of Seismic Exploration, **1**, 265–279.

Hubral, P., Schleicher, J., Tygel, M., and Hanitzsch, C., 1993, Determination of Fresnel zones from traveltimes measurement: Geophysics, **58**, 703–712.

Hubral, P., 1983, Computing true amplitude reflections in a laterally inhomogeneous earth: Geophysics, **48**, no. 8, 1051–1062.

Hubral, P., 1999, Macro-model independent seismic reflection imaging: J. Appl. Geoph., **42**, no. 3,4.

Jäger, R., 1999, The Common-Reflection Surface stack - Theory and application.: Master's thesis, University of Karlsruhe (Germany).

Schleicher, J., Tygel, M., and Hubral, P., 1993, Parabolic and hyperbolic paraxial two-point traveltimes in 3D media: Geophysical Prospecting, **41**, no. 4, 495–514.

Tegland, E. R., 1977, 3-D seismic techniques boost field development: Oil and Gas Journal, **75**, no. 37, 79–82.

Walton, G. G., 1972, Three-dimensional seismic method.: Geophysics, **37**, 417–430.